

## LUMINOSITY INDICATORS IN THE ULTRAVIOLET SPECTRA OF TYPE IA SUPERNOVAE

RYAN J. FOLEY, ALEXEI V. FILIPPENKO

Department of Astronomy, University of California, Berkeley, CA 94720-3411 (rfoley@astro.berkeley.edu, alex@astro.berkeley.edu)

AND

SAURABH W. JHA

Dept. of Physics and Astronomy, Rutgers, the State University of New Jersey, 136 Frelinghuysen Road, Piscataway, NJ 08854  
(saurabh@physics.rutgers.edu)

*Draft version November 25, 2018*

### ABSTRACT

We present a complete sample of *International Ultraviolet Explorer* and *Hubble Space Telescope* ultraviolet (UV) spectra of Type Ia supernovae (SNe Ia) through 2004. We measure the equivalent width (EW) and blueshifted velocity of the minimum of the one strong UV feature, Fe II  $\lambda$ 3250. We also quantify the slope of the near-UV spectra using a new parameter, the “UV ratio.” We find that the velocity of the Fe II line does not correlate with light-curve shape, while the EW shows distinct behavior for the slow and fast-declining objects. Using precise Cepheid and surface brightness fluctuation distance measurements of 6 objects with UV spectra observed near maximum light (a total of 12 spectra), we determine that the UV ratio at maximum light is highly correlated with SN Ia luminosity. A larger sample of UV spectra is necessary to determine the validity of these luminosity indicators and whether they can be combined with light-curve shape to improve measured SN Ia distances.

*Subject headings:* supernovae — general, individual (SNe 1980N, 1981B, 1982B, 1983G, 1986G, 1989B, 1989M, 1990M, 1990N, 1991T, 1992A, 2001ay, 2001ba, 2001eh, 2001el, 2001ep, 2001ex, 2003bf, 2003bt), cosmology — observations, distance scale

### 1. INTRODUCTION

Ultraviolet (UV) spectra of Type Ia supernovae (SNe Ia) have been incredibly helpful in understanding the explosion physics of SNe Ia (e.g., Jeffery et al. 1992); over the last 16 years, however, very few such spectra have been obtained. Compounding the problem, the demise in 2004 of the Space Telescope Imaging Spectrograph (STIS) aboard the *Hubble Space Telescope* (*HST*) has stalled progress in this field.

In addition to providing a better understanding of SN Ia explosions, UV spectra are critical for properly measuring luminosity distances of high-redshift SNe Ia, where the observed optical bands probe the rest-frame UV. Establishing the luminosity distances of SNe Ia is extremely important for many studies, including the determination of cosmological parameters such as  $H_0$ ,  $\Omega_M$ , and  $\Omega_\Lambda$  (e.g., Riess et al. 1998; Perlmutter et al. 1999; Riess et al. 2005). Despite a large intrinsic dispersion of SN Ia absolute magnitudes ( $\sigma \approx 0.7$  mag), there are ways of “correcting” this. For SNe Ia with precise and independent relative distance measurements, such as SNe Ia in the Hubble flow or those in host galaxies which have distances measured by the Cepheid period-luminosity ( $P/L$ ) relationship, one may test whether intrinsic SN features correlate with peak luminosity. Doing this, various authors have found several observables in SN light curves and spectra that correlate with luminosity (e.g., Nugent et al. 1995; Benetti et al. 2005; Wang et al. 2007). The most well-known relationship is that between the light-curve shape and luminosity (Phillips 1993). We can then use such relationships to determine the precise distances of high-redshift SNe.

Although there are many different known observables

that correlate with luminosity, thus far a combination has failed to significantly reduce the scatter in Hubble diagrams, indicating that all known luminosity indicators probe essentially the same parameter space, precluding further improvements in SN Ia distances. Since the luminosity of SNe Ia (at peak) is powered by the decay of  $^{56}\text{Ni}$  and UV spectra of SNe Ia are highly dependent on iron-peak elements, one might expect there to be correlations between observables in the UV spectrum of a SN Ia and its peak luminosity.

An indication that the UV colors might probe a different part of parameter space than the light-curve shape vs. luminosity relationship is found in the case of SNe 1992A and 1994D. Despite having very similar light-curve shapes (SN 1992A has  $\Delta m_{15}(B) = 1.33$  and SN 1994D has  $\Delta m_{15}(B) = 1.31$ ; N. Suntzeff, 2007, private communication; Richmond et al. 1995) and  $B - V$  colors, SN 1994D was  $\sim 0.3$  mag bluer than SN 1992A in the near-UV (as measured by  $U - B$ ). This shows that there are real differences among SNe Ia that do not correlate with light-curve shape and suggests that there could be a “second parameter” that may further reduce the scatter in the derived SN Ia luminosities.

With this in mind, we have examined all 64 SN Ia UV spectra observed with either the *International Ultraviolet Explorer* (*IUE*) or *HST* through 2004, when STIS became inoperable. For completeness, we also present the additional 12 SN Ia UV spectra having no available light-curve information. Using our sample of SN Ia spectra, we investigate possible correlations of the observables in the UV spectra with luminosity.

### 2. OBSERVATIONS

A total of 77 UV spectra of 20 SNe Ia were obtained with *IUE* and *HST* through 2004. Of these, there are 16 SNe Ia with available optical light curves. Most spectra were taken with *IUE*, with later spectra from *HST* using both the Faint Object Spectrograph (FOS) and STIS. Some of these data have been published elsewhere (SN 1981B, Branch & Venkatakrisna 1986; SNe 1990N, 1991T, Jeffery et al. 1992; SN 1992A, Kirshner et al. 1993; SNe 2001eh, 2001ep, Sauer et al. 2008). All data were retrieved from the *IUE* and *HST* data archives (de La Pena et al. 1994). The fully reduced data were then reprocessed to remove cosmic rays and other defects according to standard published techniques.

The photometric and host-galaxy information for each SN is listed in Table 1. When available, we have included the distance modulus for the host galaxies. Distances are derived from infrared (IR) surface brightness fluctuations (SBF), Cepheids, or directly for hosts in the Hubble flow. All distance moduli are on the IR SBF scale determined by Jensen et al. (2003), calibrated to the *HST* Key Project Cepheid scale (Freedman et al. 2001), yielding  $H_0 = 76 \text{ km s}^{-1} \text{ Mpc}^{-1}$ .

Having the distance modulus ( $\mu$ ) for each host galaxy, the visual maximum brightness and measured host-galaxy visual extinction (from MLCS2k2 Jha et al. 2007) allow one to calculate the absolute brightness of each SN at maximum light:

$$M_V = V_{\text{max}} - A_V - \mu. \quad (1)$$

To compare with the light-curve shape vs. luminosity relationship, we have also included in Table 1 two measures of light-curve shape:  $\Delta m_{15}$  (Phillips 1993) and MLCS  $\Delta$  (Riess et al. 1996; Jha et al. 2007).

There exists a single UV spectrum of the fast-declining, subluminous SN 1991bg (e.g., Filippenko et al. 1992a); however, it has such a low signal-to-noise ratio (S/N) that no clear SN signal can be discerned. It has been removed from all subsequent discussion, but is included in Tables 1 and 2 for completeness. In addition to the 15 SNe Ia (removing SN 1991bg) with available light curves, there exist four objects (SNe 1989M, 1990M, 2003bf, and 2003bt) which have UV spectra, but no available light curves. Without light curves, the phase relative to maximum brightness, light-curve shape parameters, and brightness at maximum cannot be determined; thus, these objects have been removed from further analysis. We do include these SNe in Table 1 and their spectra in Table 2 for completeness and for future studies if their light curves eventually become available.

We also provide specific information for each spectrum in Table 2, listing the UT date of observation, the telescope (and instrument) used to obtain the spectrum, the phase of the spectrum relative to maximum  $B$  brightness (when available; determined from the light curves; see Table 1), and various quantities calculated from the spectra (see § 3). The 64 spectra with phase information are presented in Figures 1–4. The 13 spectra of SNe 1989M, 1990M, 1991bg, 2003bf, and 2003bt (which have no phase information) are presented in Figure 5. All spectra compiled in this paper can be obtained online<sup>1</sup>. For all analyses, the spectra have been corrected for Galactic ex-

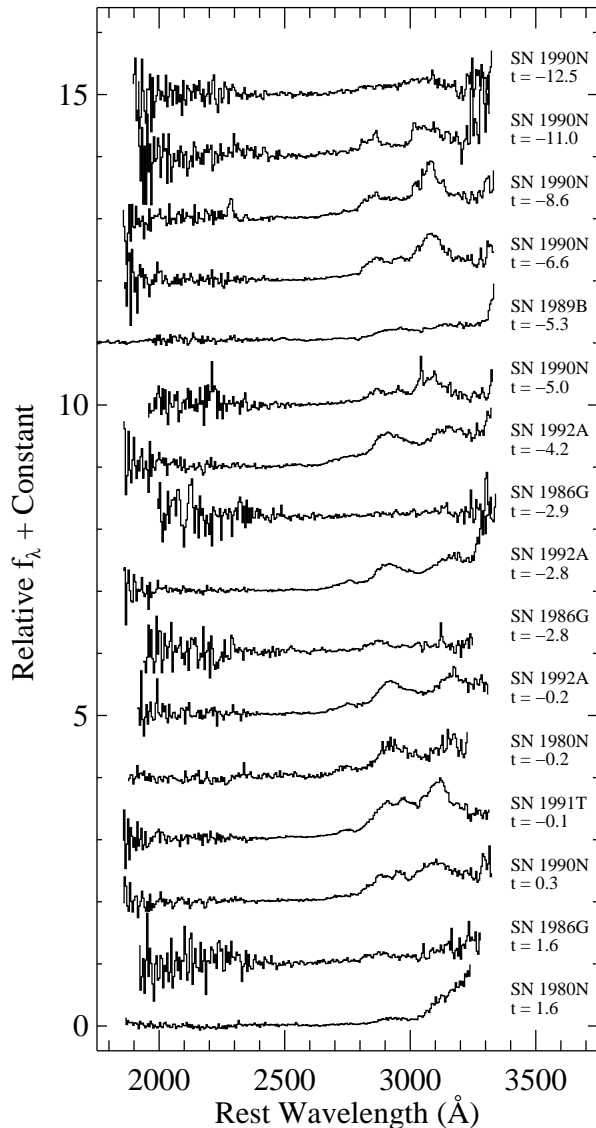


FIG. 1.— UV spectra of SNe Ia with  $t \leq 1.6$  d past maximum brightness. The spectra are generally of low S/N, but some features are apparent. In particular, there is an absorption trough at  $\sim 3000$  Å, attributed to Fe II  $\lambda 3250$  (Branch & Venkatakrisna 1986), on either side of two peaks. These features are seen in nearly every spectrum with  $t < 3$  weeks and of reasonable S/N.

tingtion (Schlegel et al. 1998), and  $R_V = 3.1$  has been assumed for both Milky Way and host-galaxy extinction.

### 3. ANALYSIS

#### 3.1. Line Features

Although the optical maximum-light spectra of SNe Ia are dominated mainly by intermediate-mass elements (e.g., Ca, Si, S; see Filippenko 1997, for a review), the UV maximum-light spectrum is dominated by Fe-peak elements. An analysis of the  $t = 5$  d spectrum of SN 1992A has revealed many complex, low-amplitude line features (Kirshner et al. 1993), but for almost all of our sample the S/N is too low to detect them. We do, however, detect the prominent trough at  $\sim 3000$  Å, attributed to Fe II  $\lambda 3250$  (Branch & Venkatakrisna 1986), in nearly all of our spectra having sufficiently high S/N at  $t < 3$  weeks

<sup>1</sup> <http://astro.berkeley.edu/~rfoley/uvspectra/>.

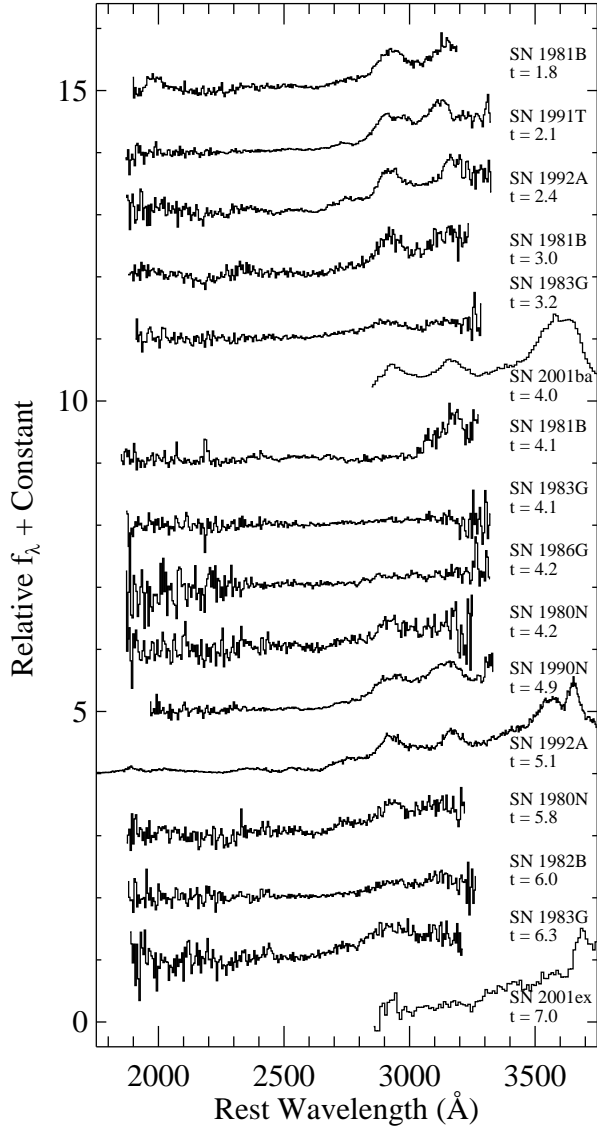


FIG. 2.— Same as Figure 1, except with  $1.8 \leq t \leq 7.0$  d past maximum.

(Fig. 1–4). Being the strongest feature in the near-UV spectra of SNe Ia, we are able to measure its velocity and equivalent width (EW) in most of our data.

We fit a Gaussian profile to the Fe II feature to measure its velocity. Since the S/N of the spectra is relatively low, we also use the Gaussian fits to measure the EW of the Fe II line. To properly measure the Fe II EWs, we must choose wavelength regions to act as the continuum. For this, we select the median value from the peaks just blueward and redward of the line (an example can be seen in Figure 6). These regions are different for each spectrum and are somewhat subjective. Consequently, the systematic errors associated with any given measurement may be as large as  $10 \text{ \AA}$ .

In Figure 7, we present the Fe II line velocity as a function of time for our sample. We assume that the Fe II feature has a  $gf$ -weighted rest-frame wavelength of  $3250 \text{ \AA}$  (D. Branch, 2007, private communication). Although the exact rest-frame wavelength of the line

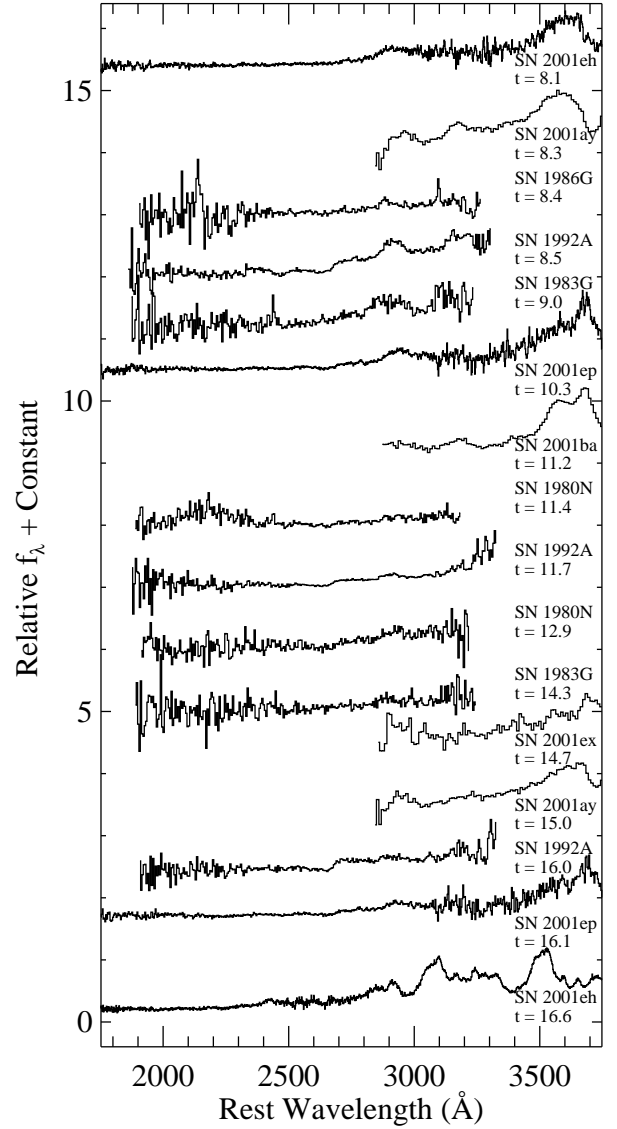


FIG. 3.— Same as Figure 1, except with  $8.1 \leq t \leq 16.6$  d past maximum.

may be slightly different from this value, it is not important for examining general trends and comparing objects. For the Fe II feature, we see that the velocity decreases significantly from premaximum to maximum light for SNe 1986G and 1990N, while the velocity change is relatively flat for SNe 1992A. The velocity gradient is relatively shallow after maximum brightness. With few pre-maximum spectra, we are unable to definitively say whether the velocity gradient for typical SNe Ia decreases with time similar to the velocity evolution of optical lines from intermediate-mass elements (e.g., Patat et al. 1996; Benetti et al. 2005) or if the velocity gradient is flatter. We do not see any trends in the velocity evolution that correlate with light-curve shape.

As seen in Figure 8, the Fe II EWs are significantly different from object to object. Moreover, there is no definitive trend among the entire sample for the evolution of the line with time. For example, the EW in SN 1980N increases from around maximum brightness for about a

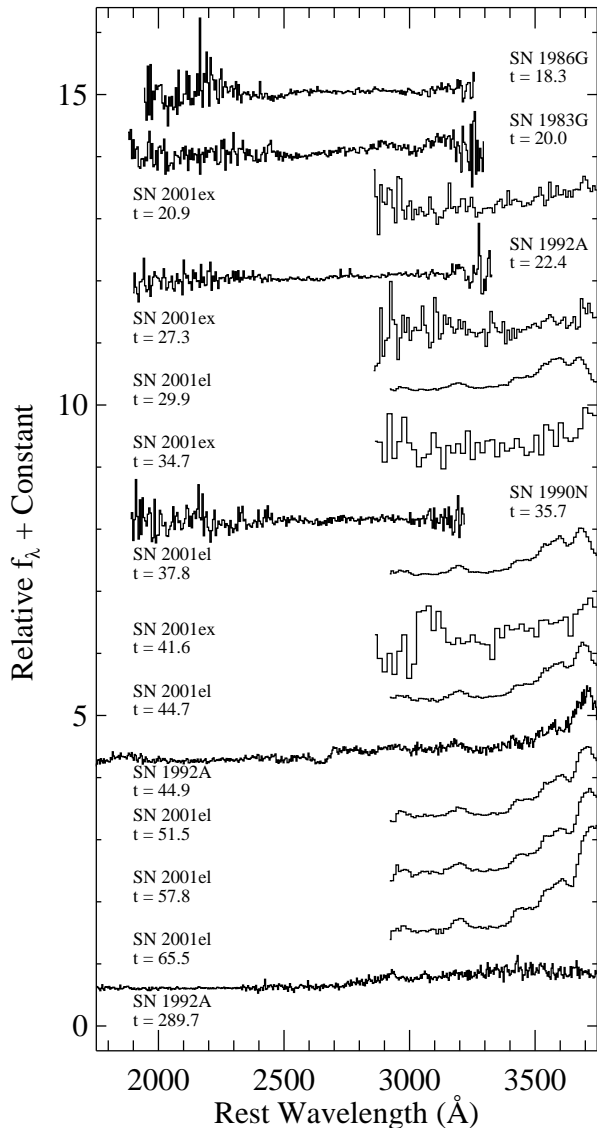


FIG. 4.— Same as Figure 1, except with  $t \geq 18.3$  d past maximum.

week, then falls dramatically (87% over 1.6 d), only to climb to its previous level about a month after maximum brightness.

However, separating the objects by light-curve shape does reveal some differences among the subsamples. On average, the low- $\Delta$  (slow-declining light curve, high-luminosity) objects have lower EWs near maximum, and for the single object with several pre-maximum epochs, the EW appears to decline with time before maximum brightness. The high- $\Delta$  (fast-declining light curve, low-luminosity) objects, on the other hand, have larger EWs near maximum brightness, and the strength of the line appears to increase with time from before maximum until after maximum. The normal-luminosity events do not appear to follow any particular trend, but their EWs tend to fall between the high and low- $\Delta$  objects at maximum brightness.

### 3.2. UV Spectral Shape and Absolute Magnitude

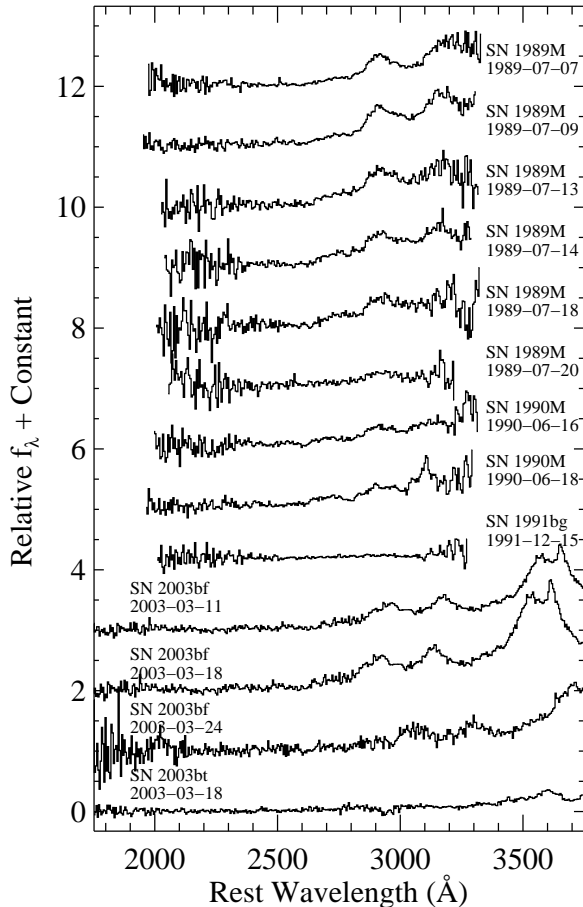


FIG. 5.— UV spectra of SNe Ia with no phase information. UT dates of observation are given. We also include a spectrum of SN 1991bg, taken at  $t = 2.4$  d, but with no discernible signal.

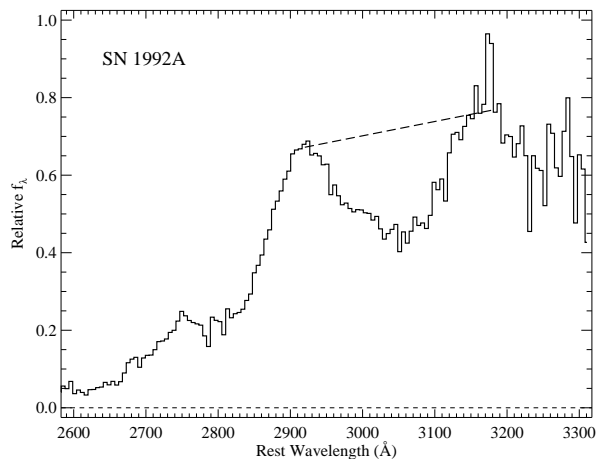


FIG. 6.— UV spectrum of SN 1992A at  $t = -0.2$  d. An example of the choice of the continuum placement for measuring the EW of Fe II  $\lambda 3250$  is shown.

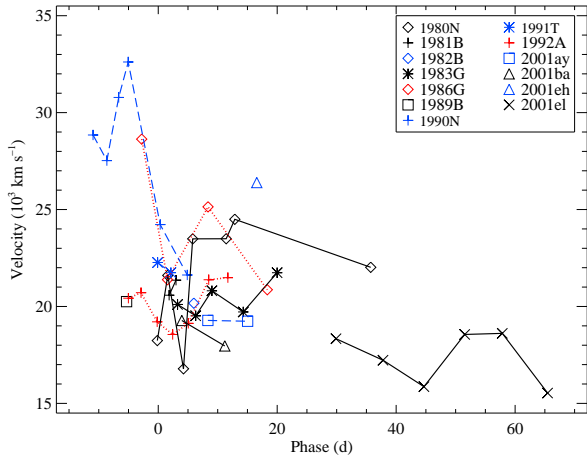


FIG. 7.— The blueshifted velocity of the minimum of the Fe II feature as a function of time for various SNe Ia assuming a rest-frame  $gf$ -weighted wavelength of  $3250 \text{ \AA}$  for Fe II. The normal, high, and low- $\Delta$  (corresponding to normal, low, and high luminosity) objects are shown in black, red, and blue (with solid, dotted, and dashed lines connecting points), respectively.

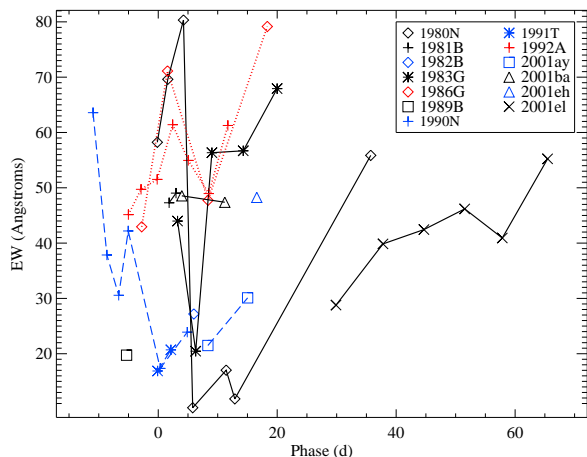


FIG. 8.— The EW of the Fe II feature as a function of time for various SNe Ia. The normal, high, and low- $\Delta$  (corresponding to normal, low, and high luminosity) objects are shown in black, red, and blue (with solid, dotted, and dashed lines connecting points), respectively.

Examining the UV spectra, we see that the overall spectral shape differs dramatically among various objects. Some objects have strong continua at  $\sim 3200 \text{ \AA}$ , only to drop rapidly by  $\sim 2600 \text{ \AA}$ , while others have a much shallower decline from long to short wavelengths. Figure 9 shows spectra of SNe 1991T and 1992A at maximum light. It is clear that SN 1991T has excess flux relative to SN 1992A in the range  $2900 \lesssim \lambda \lesssim 3100 \text{ \AA}$ .

Although there are many ways to characterize the spectral slope (such as fitting a straight line to the flux density), we determined that differences in spectral features prevent an accurate assessment of the slope with most of these methods. One method which can avoid spectral features (to a large degree) is to measure the ratio of the flux density at two separate wavelengths. For this, we have chosen wavelengths of  $2770 \text{ \AA}$  and  $2900 \text{ \AA}$ , which correspond to parts of the spectra that have reason-

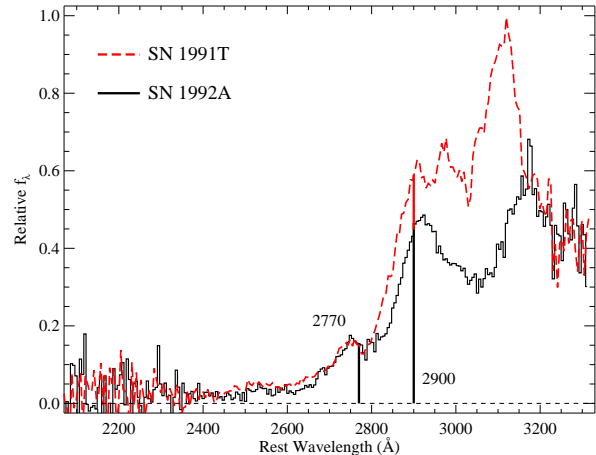


FIG. 9.— UV spectrum of SN 1992A at  $t = -0.2 \text{ d}$  (black) and SN 1991T at  $t = -0.1 \text{ d}$  (red) normalized to have the same flux at  $2770 \text{ \AA}$ . The fluxes measured at  $2770 \text{ \AA}$  and  $2900 \text{ \AA}$  are shown. SN 1991T has a smaller UV ratio (see Eq. 3) than SN 1992A.

able S/N and avoid major features in the near-maximum ( $-3 \leq t \leq 3 \text{ d}$ ) spectra. We define the “UV ratio” as

$$\mathcal{R}_{UV} = f_{\lambda}(2770 \text{ \AA})/f_{\lambda}(2900 \text{ \AA}). \quad (2)$$

For  $f_{\lambda}(2770 \text{ \AA})$  and  $f_{\lambda}(2900 \text{ \AA})$ , we measure the median flux density in the  $40 \text{ \AA}$  regions centered on  $2770 \text{ \AA}$  and  $2900 \text{ \AA}$ , respectively. Figure 9 demonstrates this method with SNe 1991T and 1992A. We also calculate an uncertainty for this ratio by measuring all flux-density ratios within a  $20 \text{ \AA}$  region centered on each wavelength value ( $\pm 10 \text{ \AA}$ ) and with the same wavelength spacing to achieve a corresponding slope [e.g.,  $f_{\lambda}(2760 \text{ \AA})/f_{\lambda}(2890 \text{ \AA})$ ,  $f_{\lambda}(2765 \text{ \AA})/f_{\lambda}(2895 \text{ \AA})$ ,  $f_{\lambda}(2780 \text{ \AA})/f_{\lambda}(2910 \text{ \AA})$ ]. The UV ratio and its uncertainty are presented in Table 2 for all objects covering the wavelength range  $2750\text{--}2920 \text{ \AA}$ .

We chose the range  $-3 < t < 3 \text{ d}$  so that the features do not shift dramatically from one spectrum to another causing the adopted fixed wavelengths to correspond to different physical features. If we expand the range of phases to  $\pm 7 \text{ d}$ , the relationships presented below remain, but with increased scatter.

In Figure 10, we see that the UV ratio and  $\Delta$  are highly correlated (correlation coefficient of 0.900). Objects that decline slowly (small  $\Delta$ ) have small UV ratios, while those that fade rapidly (large  $\Delta$ ) have large UV ratios. This is similar to stating that SNe Ia with slow-declining light curves have redder spectra between  $2770 \text{ \AA}$  and  $2900 \text{ \AA}$  than those with fast-declining light curves. This is opposite to the trend in optical colors, where SNe Ia with slow-declining light curves have bluer  $U - B$  and  $B - V$  than those with fast-declining light curves.

In Figure 11, we show the UV ratio of 12 spectra (from 6 objects: SNe 1980N, 1981B, 1986G, 1990N, 1991T, and 1992A) with  $-3 \leq t \leq 3 \text{ d}$  compared to  $M_V$  at maximum light for the SNe. Spectra of more recent SNe Ia tend to have  $t > 3 \text{ d}$ , and several barely probe the UV, not reaching  $2770 \text{ \AA}$ . We find that the UV ratio is highly correlated with the peak absolute magnitude of the SN, with correlation coefficients of 0.811 and 0.860 for the individual UV ratio measurements for each spectrum and

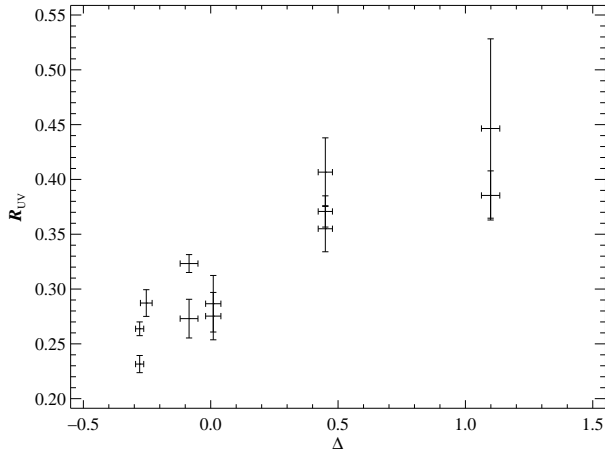


FIG. 10.— Relationship between the UV ratio and  $\Delta$  for spectra with  $-3 < t < 3$  d.

the averaged UV ratio measurements for each object, respectively. By averaging the UV ratio for each object (to weight all objects equally), we have fit a line to the data, yielding the relationship

$$M_V(t = 0) = -19.165 + 6.293(\mathcal{R}_{UV} - 0.3) \text{ mag} \quad (3)$$

with a residual scatter of 0.207 mag.

The measurement of  $\mathcal{R}_{UV}$  is affected by dust reddening along the line of sight (both from our Galaxy and the SN host galaxy). Though this can be significant in the near-UV, the small wavelength range over which we measure  $\mathcal{R}_{UV}$  (only 130 Å) makes it rather insensitive to extinction. In Figure 12, we show the effect of dust reddening on the measurement of  $\mathcal{R}_{UV}$ , and find that a  $\pm 0.6$  mag change in  $A_V$  yields less than a 10% change in  $\mathcal{R}_{UV}$  (for any  $R_V \geq 2.0$ ). Of the sample presented here, only SN 1986G, which has  $A_V = 2.313$  mag (as measured from MLCS, assuming  $R_V = 3.1$ ; for lower values of  $R_V$ ,  $A_V$  also decreases), has a UV ratio significantly affected by extinction. If we were to ignore this effect, we would have derived

$$M_V(t = 0) = -19.105 + 6.527(\mathcal{R}_{UV(\text{Uncor})} - 0.3) \text{ mag}, \quad (4)$$

differing little from the relation in Eq. 3.

### 3.3. Reducing the Scatter in the SN Ia Hubble Diagram

As mentioned previously, combining various luminosity indicators has failed to reduce the scatter in SN Ia Hubble diagrams. Therefore, a single parameter can characterize the luminosity of a SN Ia.

Jha et al. (2007) derived  $M_V$  as a quadratic function of  $\Delta$ . Since our sample is different from the Hubble-flow sample used to create the relationship, and the relationship of Jha et al. (2007) is nearly linear, and we only have 6 objects with measured  $\mathcal{R}_{UV}$  and  $-3 \leq t \leq 3$  d, we decided to fit for a new, linear relationship. Excluding SN 1986G from our fits based on its large and uncertain host-galaxy reddening, we find

$$M_V(t = 0) = -19.118 + 1.020\Delta \text{ mag}. \quad (5)$$

This relationship has  $\chi^2$  per degree of freedom (dof) = 5.771/3, a reasonable, but not excellent, fit. Using the

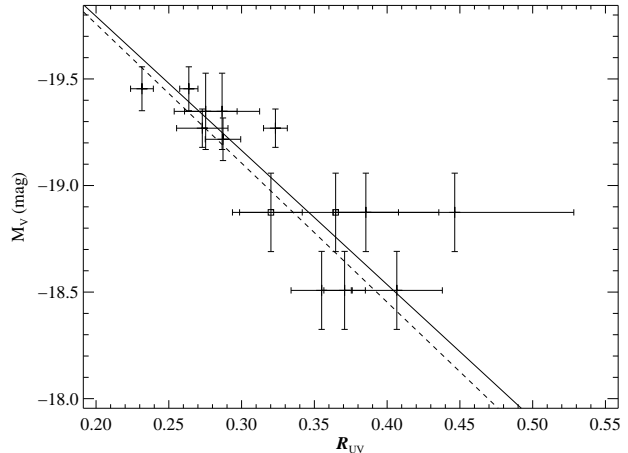


FIG. 11.— The UV ratio compared to the absolute magnitude at maximum for several SNe Ia. The square points are the values for SN 1986G if no host-galaxy reddening correction is applied to the spectrum before calculating  $\mathcal{R}_{UV}$  (an extinction correction is still applied to its measured absolute magnitude). The solid line is the fit for the host-galaxy extinction corrected spectra, described by  $M_V = -19.165 + 6.293(\mathcal{R}_{UV} - 0.3)$  mag, where  $\mathcal{R}_{UV}$  is the UV flux ratio. The dashed line is the fit for the uncorrected spectra, described by  $M_V = -19.105 + 6.527(\mathcal{R}_{UV} - 0.3)$  mag.

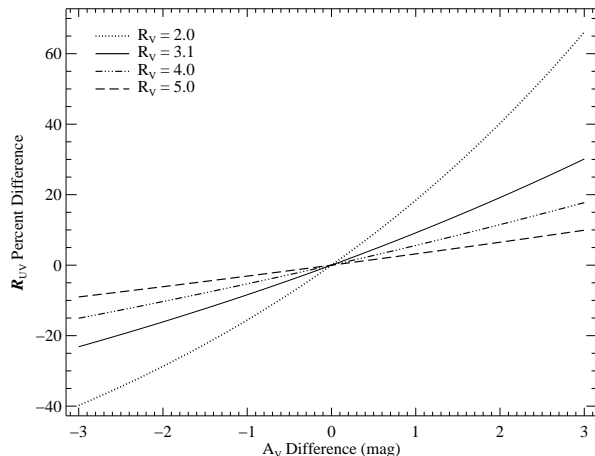


FIG. 12.— The percent difference of the UV ratio as a function of  $A_V$  for different values of  $R_V$ . Negative values of  $A_V$  are shown in case the extinction is overestimated. For  $R_V = 3.1$  ( $R_V = 2.0$ ), there is less than a 10% difference for  $-1.20 < A_V < 1.08$  mag ( $-0.66 < A_V < 0.60$ ).

absolute magnitudes from this new relationship, we find a scatter in the residuals to the absolute-magnitude fit of 0.167 mag, which is slightly lower than, but similar to 0.18 mag, the scatter in the Hubble diagram using the results of Jha et al. (2007).

If we then include the UV ratio,  $\mathcal{R}_{UV}$ , in the fit, we find

$$M_V(t = 0) = -19.161 + 0.043\Delta + 6.578(\mathcal{R}_{UV} - 0.3) \text{ mag}. \quad (6)$$

This relationship has  $\chi^2/\text{dof} = 2.155/2$ , which is much improved from the relationship given in Eq. 5. The residual scatter also decreases to 0.090 mag. The low scatter (the mean error for the absolute magnitudes is 0.140 mag) indicates that the data may be slightly over-

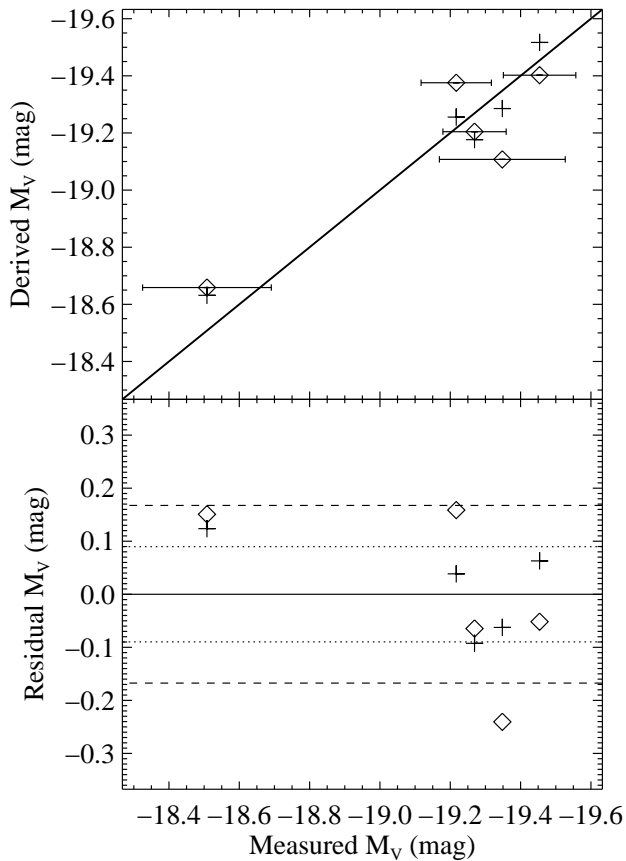


FIG. 13.— (*top panel*): Derived absolute magnitudes using Eq. 5 (diamonds) and Eq. 6 (crosses), which do not and do include the UV ratio, respectively. The uncertainties in the measured  $M_V$  values are shown. (*bottom panel*): The residual absolute magnitudes from the relationships. The dashed and dotted lines show the standard deviation of the residuals from Eq. 5 and Eq. 6, respectively.

fit, requiring more data to determine if this relationship is valid. Eq. 6 shows that  $\mathcal{R}_{UV}$  is more influential on the determination of  $M_V$  than  $\Delta$ . In fact, fitting a relationship between just  $M_V$  and  $\mathcal{R}_{UV}$  (and removing SN 1986G from the sample) gives  $\chi^2/\text{dof} = 2.166/3$ . It is obvious that we need a larger sample to determine if  $\mathcal{R}_{UV}$  is in the same family of luminosity indicators as light-curve shape.

Figure 13 shows the derived absolute magnitudes (and residuals) from Eqs. 5 and 6 for our sample of objects with near-maximum spectra.

## 4. DISCUSSION AND CONCLUSIONS

### 4.1. The Fe II Feature

Based on the very small sample of SNe Ia with available UV spectra and optical light curves, we are able to see general trends regarding the evolution of the strong Fe II  $\lambda 3250$  feature. The line velocity and its evolution do not appear to differ significantly among objects with different light-curve shapes. On the other hand, the strength near maximum light and evolution of the EW of the line do appear to depend on the subsample, with fast-declining objects having a larger EW near maximum light than slow-declining objects.

The variation in EW measurements for these subsamples is similar to the difference in the EW of the Si II

$\lambda 5972$  line seen in SN 1991T-like and SN 1991bg-like objects (e.g., Filippenko et al. 1992a,b), and may be another indication of luminosity.

The trend between the slope of the UV continuum (i.e., the UV ratio) and the absolute magnitude of the SN, with brighter objects having a steeper decline to shorter wavelengths, is similar to stating that more-luminous objects have brighter near-UV flux. The difference between Fe II EWs for the slow and fast-declining objects may simply be a higher continuum in the slow-declining objects. Similarly, SN 1991T and its brethren have hot photospheres which ionize Fe to Fe III, and at maximum light they have strong Fe III features and absent Fe II features, which are present in normal-luminosity SNe Ia (e.g., Filippenko et al. 1992b). The Fe II  $\lambda 3250$  feature may be weaker in the UV spectra of SN 1991T-like objects because most of the Fe has been ionized to Fe III. Since the UV continuum is blanketed by Fe II lines, the Fe II/Fe III ratio may be the reason for the differences in both the Fe II EW and UV ratio.

### 4.2. The UV Continuum

We have shown that for our small sample, there is a relationship between the near-UV spectral slope, described by our “UV ratio,” and the luminosity of SNe Ia. For a given SN Ia, the luminosity is derived from a combination of distance moduli from independent sources, a measured peak apparent magnitude, and a calculated extinction. The UV slope is measured from the spectrum of a SN. Since these two observations are independent, it is very intriguing that we are able to find a strong correlation between them. This new luminosity indicator might turn out to be particularly useful for high-redshift objects where it is difficult to observe the rest-frame optical light.

We show that slow-declining SNe Ia have redder near-UV colors (as measured by the UV ratio) than fast-declining SNe Ia. Jha et al. (2006) found that slow-declining SNe Ia have bluer  $U - B$  colors than fast-declining SNe Ia. This difference suggests that the near UV, in particular  $\sim 2800\text{--}4000 \text{ \AA}$ , may be very sensitive to luminosity, with bright, slow-declining SNe Ia having a larger flux density in this region compared to faster-declining objects. This would lead to both redder  $\mathcal{R}_{UV}$  values and bluer  $U - B$  colors. Combining this result with recent studies of the variation in SN Ia ground-based near-UV spectra (Foley et al. 2007; Ellis et al. 2008) may suggest that the region strongly correlated with luminosity might be restricted to the range  $\sim 2800\text{--}3500 \text{ \AA}$ .

We also present the possibility that the relationship between the UV ratio and luminosity may represent a new vector in the multi-dimensional SN Ia luminosity parameter space. This possible “second parameter” might open the door for more precise distances to high-redshift SNe Ia, significantly improving our measurements of cosmological parameters, such as the equation-of-state parameter of the dark energy,  $w = P/(\rho c^2)$ , and its derivatives.

### 4.3. Future Studies

One way to test the validity of the UV ratio as a luminosity indicator is to measure a similar photometric color. The wavelengths we chose for this study, 2770

and 2900 Å, are very closely spaced, and it is difficult to probe flux densities at these wavelengths independently. However, the low S/N of our spectra prevented us from probing wavelengths shortward of 2600 Å, and the UV spectra rarely included wavelengths redward of 3300 Å. Use of longer or shorter wavelengths may provide a similar (or potentially better) relationship. However, widely separated wavelengths make the results more sensitive to errors in the adopted reddening.

There are currently several SNe Ia that have been observed photometrically in the UV with the *UVOT* instrument on *Swift*. Its UVW2, UVM2, and UVW1 filters have effective wavelengths of 1900, 2200, and 2600 Å, respectively. Either a UVM2 – UVW1 or UVW1 – U color may result in a similar relationship. We do note, however, that the UVW1 and UVW2 filters have long red tails in their response functions; combined with the rapidly increasing flux of a SN Ia to the red, this may increase the observed scatter in the relationship.

Additional high-S/N spectra of SNe Ia with *HST* or *Swift* (which can obtain very early epochs) in host galaxies having precise relative distances are also necessary to test this relationship. The small sample of 6 SNe Ia with available maximum-light UV spectra and optical light curves provides a glimpse of the potential UV spectra have in determining SN Ia distances. It may be that this relationship is a statistical fluke; however, the light-curve shape vs. luminosity relationship was first clearly measured with a sample of only 7 objects (removing SNe 1986G and 1989B from a set of 9 because of their uncertain reddening; Phillips 1993). This gives us hope that with a larger sample, the relationship will improve and provide even better SN Ia distances. With the anticipated repair of STIS aboard *HST*, or at least with the installation of the Cosmic Origins Spectrograph (COS), soon it should again be possible to obtain high-quality

UV spectra of SNe Ia.

Most past and present high-redshift SN surveys have obtained limited and typically poor rest-frame UV spectra for high-redshift SNe Ia. Currently there is no public database of high-redshift SN Ia spectra for which we can apply this method and test its validity at high redshifts. Ellis et al. (2008) present a large sample of high-S/N SN Ia spectra, including 12 objects which have spectra at  $-3 \leq t \leq 3$  d. This, or a similar sample, would be excellent for testing this method.

Looking forward, the Joint Dark Energy Mission (JDEM) will find and follow several thousand SNe Ia out to  $z \approx 2$ . Incorporating rest-frame UV photometry and spectroscopy into both mission planning and analysis may help produce the requisite precision necessary to achieve its mission objectives.

We are grateful to D. Branch for revisiting research he performed over 20 years ago. All of the data presented in this paper were obtained from the Multimission Archive at the Space Telescope Science Institute (MAST), including observations made with the NASA/ESA *Hubble Space Telescope*. STScI is operated by the Association of Universities for Research in Astronomy, Inc., under NASA contract NAS5-26555. Support for MAST for non-*HST* data is provided by the NASA Office of Space Science via grant NAG5-7584 and by other grants and contracts. Our work is supported by NSF grant AST-0607485, as well as by NASA/*HST* grant GO-10182 from STScI. This research has made extensive use of the NASA/IPAC Extragalactic Database (NED), which is operated by the Jet Propulsion Laboratory, California Institute of Technology, under contract with NASA.

*Facilities: IUE, HST: FOS, STIS*

## REFERENCES

- Altavilla, G., Fiorentino, G., Marconi, M., Musella, I., Cappellaro, E., Barbon, R., Benetti, S., Pastorello, A., Riello, M., Turatto, M., & Zampieri, L. 2004, *MNRAS*, 349, 1344
- Benetti, S., Cappellaro, E., Mazzali, P. A., Turatto, M., Altavilla, G., Bufano, F., Elias-Rosa, N., Kotak, R., Pignata, G., Salvo, M., & Stanishev, V. 2005, *ApJ*, 623, 1011
- Branch, D. & Venkatakrisna, K. L. 1986, *ApJ*, 306, L21
- Buta, R. J., Corwin, Jr., H. G., & Opal, C. B. 1985, *PASP*, 97, 229
- Buta, R. J. & Turner, A. 1983, *PASP*, 95, 72
- Ciatti, F., Barbon, R., Cappellaro, E., & Rosino, L. 1988, *A&A*, 202, 15
- de La Pena, M. D., Nichols-Bohlin, J., Levay, K. L., & Michalitsianos, A. 1994, *Astronomical Data Analysis Software and Systems*, 3, 127
- Ellis, R. S., Sullivan, M., Nugent, P. E., Howell, D. A., Gal-Yam, A., Astier, P., Balam, D., Bolland, C., Basa, S., Carlberg, R. G., Conley, A., Fouchez, D., Guy, J., Hardin, D., Hook, I., Pain, R., Perrett, K., Pritchet, C. J., & Regnault, N. 2008, *ApJ*, 674, 51
- Filippenko, A. V. 1997, *ARA&A*, 35, 309
- Filippenko, A. V., Richmond, M. W., Branch, D., Gaskell, M., Herbst, W., Ford, C. H., Treffers, R. R., Matheson, T., Ho, L. C., Dey, A., Sargent, W. L. W., Small, T. A., & van Breugel, W. J. M. 1992a, *AJ*, 104, 1543
- Filippenko, A. V., Richmond, M. W., Matheson, T., Shields, J. C., Burbidge, E. M., Cohen, R. D., Dickinson, M., Malkan, M. A., Nelson, B., Pietz, J., Schlegel, D., Schmeer, P., Spinrad, H., Steidel, C. C., Tran, H. D., & Wren, W. 1992b, *ApJ*, 384, L15
- Foley, R. J., Filippenko, A. V., Aguilera, C., Becker, A. C., Blondin, S., Challis, P., Clocchiatti, A., Covarrubias, R., Davis, T. M., Garnavich, P. M., Jha, S., Kirshner, R. P., Krisciunas, K., Leibundgut, B., Li, W., Matheson, T., Miceli, A., Miknaitis, G., Pignata, G., Rest, A., Riess, A. G., Schmidt, B. P., Smith, R. C., Sollerman, J., Spyromilio, J., Stubbs, C. W., Tonry, J. L., Suntzeff, N. B., Wood-Vasey, W. M., & Zenteno, A. 2007, *ArXiv e-prints*, 0710.2338
- Freedman, W. L., Madore, B. F., Gibson, B. K., Ferrarese, L., Kelson, D. D., Sakai, S., Mould, J. R., Kennicutt, Jr., R. C., Ford, H. C., Graham, J. A., Huchra, J. P., Hughes, S. M. G., Illingworth, G. D., Macri, L. M., & Stetson, P. B. 2001, *ApJ*, 553, 47
- Ganeshalingam, M. et al. 2008, in prep.
- Gibson, B. K., Stetson, P. B., Freedman, W. L., Mould, J. R., Kennicutt, Jr., R. C., Huchra, J. P., Sakai, S., Graham, J. A., Fasset, C. I., Kelson, D. D., Ferrarese, L., Hughes, S. M. G., Illingworth, G. D., Macri, L. M., Madore, B. F., Sebo, K. M., & Silbermann, N. A. 2000, *ApJ*, 529, 723
- Hamuy, M., Phillips, M. M., Maza, J., Wischnjewsky, M., Uomoto, A., Landolt, A. U., & Khatwani, R. 1991, *AJ*, 102, 208
- Jeffery, D. J., Leibundgut, B., Kirshner, R. P., Benetti, S., Branch, D., & Sonneborn, G. 1992, *ApJ*, 397, 304
- Jensen, J. B., Tonry, J. L., Barris, B. J., Thompson, R. I., Liu, M. C., Rieke, M. J., Ajhar, E. A., & Blakeslee, J. P. 2003, *ApJ*, 583, 712



- Jha, S., Kirshner, R. P., Challis, P., Garnavich, P. M., Matheson, T., Soderberg, A. M., Graves, G. J. M., Hicken, M., Alves, J. F., Arce, H. G., Balog, Z., Barmby, P., Barton, E. J., Berlind, P., Bragg, A. E., Briceño, C., Brown, W. R., Buckley, J. H., Caldwell, N., Calkins, M. L., Carter, B. J., Concannon, K. D., Donnelly, R. H., Eriksen, K. A., Fabricant, D. G., Falco, E. E., Fiore, F., Garcia, M. R., Gómez, M., Grogan, N. A., Groner, T., Groot, P. J., Haisch, Jr., K. E., Hartmann, L., Hergenrother, C. W., Holman, M. J., Huchra, J. P., Jayawardhana, R., Jerius, D., Kannappan, S. J., Kim, D.-W., Kleyna, J. T., Kochanek, C. S., Koranyi, D. M., Krockenberger, M., Lada, C. J., Luhman, K. L., Luu, J. X., Macri, L. M., Mader, J. A., Mahdavi, A., Marengo, M., Marsden, B. G., McLeod, B. A., McNamara, B. R., Megeath, S. T., Moraru, D., Mossman, A. E., Muench, A. A., Muñoz, J. A., Muzerolle, J., Naranjo, O., Nelson-Patel, K., Pahre, M. A., Patten, B. M., Peters, J., Peters, W., Raymond, J. C., Rines, K., Schild, R. E., Sobczak, G. J., Spahr, T. B., Stauffer, J. R., Stefanik, R. P., Szentgyorgyi, A. H., Tollestrup, E. V., Väisänen, P., Vikhlinin, A., Wang, Z., Willner, S. P., Wolk, S. J., Zajak, J. M., Zhao, P., & Stanek, K. Z. 2006, *AJ*, 131, 527
- Jha, S., Riess, A. G., & Kirshner, R. P. 2007, *ApJ*, 659, 122
- Kirshner, R. P., Jeffery, D. J., Leibundgut, B., Challis, P. M., Sonneborn, G., Phillips, M. M., Suntzeff, N. B., Smith, R. C., Winkler, P. F., Winge, C., Hamuy, M., Hunter, D. A., Roth, K. C., Blades, J. C., Branch, D., Chevalier, R. A., Fransson, C., Panagia, N., Wagoner, R. V., Wheeler, J. C., & Harkness, R. P. 1993, *ApJ*, 415, 589
- Krisciunas, K., Suntzeff, N. B., Candia, P., Arenas, J., Espinoza, J., Gonzalez, D., Gonzalez, S., Höflich, P. A., Landolt, A. U., Phillips, M. M., & Pizarro, S. 2003, *AJ*, 125, 166
- Krisciunas, K., Suntzeff, N. B., Phillips, M. M., Candia, P., Prieto, J. L., Antezana, R., Chassagne, R., Chen, H.-W., Dickinson, M., Eisenhardt, P. R., Espinoza, J., Garnavich, P. M., González, D., Harrison, T. E., Hamuy, M., Ivanov, V. D., Krzeminski, W., Kulesa, C., McCarthy, P., Moro-Martín, A., Muena, C., Noriega-Crespo, A., Persson, S. E., Pinto, P. A., Roth, M., Rubenstein, E. P., Stanford, S. A., Stringfellow, G. S., Zapata, A., Porter, A., & Wischnjewsky, M. 2004, *AJ*, 128, 3034
- Leibundgut, B., Kirshner, R. P., Phillips, M. M., Wells, L. A., Suntzeff, N. B., Hamuy, M., Schommer, R. A., Walker, A. R., Gonzalez, L., Ugarte, P., Williams, R. E., Williger, G., Gomez, M., Marzke, R., Schmidt, B. P., Whitney, B., Coldwell, N., Peters, J., Chaffee, F. H., Foltz, C. B., Rehner, D., Siciliano, L., Barnes, T. G., Cheng, K.-P., Hintzen, P. M. N., Kim, Y.-C., Maza, J., Parker, J. W., Porter, A. C., Schmidtke, P. C., & Sonneborn, G. 1993, *AJ*, 105, 301
- Lira, P., Suntzeff, N. B., Phillips, M. M., Hamuy, M., Maza, J., Schommer, R. A., Smith, R. C., Wells, L. A., Avilés, R., Baldwin, J. A., Elias, J. H., González, L., Layden, A., Navarrete, M., Ugarte, P., Walker, A. R., Williger, G. M., Baganoff, F. K., Crotts, A. P. S., Rich, R. M., Tyson, N. D., Dey, A., Guhathakurta, P., Hibbard, J., Kim, Y.-C., Rehner, D. M., Siciliano, E., Roth, J., Seitzer, P., & Williams, T. B. 1998, *AJ*, 115, 234
- Nugent, P., Phillips, M., Baron, E., Branch, D., & Hauschildt, P. 1995, *ApJ*, 455, L147
- Patat, F., Benetti, S., Cappellaro, E., Danziger, I. J., della Valle, M., Mazzali, P. A., & Turatto, M. 1996, *MNRAS*, 278, 111
- Perlmutter, S., Aldering, G., Goldhaber, G., Knop, R. A., Nugent, P., Castro, P. G., Deustua, S., Fabbro, S., Goobar, A., Groom, D. E., Hook, I. M., Kim, A. G., Kim, M. Y., Lee, J. C., Nunes, N. J., Pain, R., Pennypacker, C. R., Quimby, R., Lidman, C., Ellis, R. S., Irwin, M., McMahon, R. G., Ruiz-Lapuente, P., Walton, N., Schaefer, B., Boyle, B. J., Filippenko, A. V., Matheson, T., Fruchter, A. S., Panagia, N., Newberg, H. J. M., & Couch, W. J. 1999, *ApJ*, 517, 565
- Phillips, M. M. 1993, *ApJ*, 413, L105
- Phillips, M. M., Phillips, A. C., Heathcote, S. R., Blanco, V. M., Geisler, D., Hamilton, D., Suntzeff, N. B., Jablonski, F. J., Steiner, J. E., Cowley, A. P., Schmidtke, P., Wyckoff, S., Hutchings, J. B., Tonry, J., Strauss, M. A., Thorstensen, J. R., Honey, W., Maza, J., Ruiz, M. T., Landolt, A. U., Uomoto, A., Rich, R. M., Grindlay, J. E., Cohn, H., Smith, H. A., Lutz, J. H., Lavery, R. J., & Saha, A. 1987, *PASP*, 99, 592
- Richmond, M. W., Treffers, R. R., Filippenko, A. V., Van Dyk, S. D., Paik, Y., Peng, C., Marschall, L. A., Laaksonen, B. D., Macintosh, B., & McLean, I. S. 1995, *AJ*, 109, 2121
- Riess, A. G., Filippenko, A. V., Challis, P., Clocchiatti, A., Diercks, A., Garnavich, P. M., Gilliland, R. L., Hogan, C. J., Jha, S., Kirshner, R. P., Leibundgut, B., Phillips, M. M., Reiss, D., Schmidt, B. P., Schommer, R. A., Smith, R. C., Spyromilio, J., Stubbs, C., Suntzeff, N. B., & Tonry, J. 1998, *AJ*, 116, 1009
- Riess, A. G., Li, W., Stetson, P. B., Filippenko, A. V., Jha, S., Kirshner, R. P., Challis, P. M., Garnavich, P. M., & Chornock, R. 2005, *ApJ*, 627, 579
- Riess, A. G., Press, W. H., & Kirshner, R. P. 1996, *ApJ*, 473, 88
- Sauer, D. N., Mazzali, P. A., Blondin, S., Filippenko, A. V., Benetti, S., Stehle, M., Challis, P., Kirshner, R. P., & Li, W. 2008, *ArXiv e-prints*, 0803.0871
- Schlegel, D. J., Finkbeiner, D. P., & Davis, M. 1998, *ApJ*, 500, 525
- Tonry, J. L., Dressler, A., Blakeslee, J. P., Ajhar, E. A., Fletcher, A. B., Luppino, G. A., Metzger, M. R., & Moore, C. B. 2001, *ApJ*, 546, 681
- Tsvetkov, D. Y. 1982, *Pis ma Astronomicheskii Zhurnal*, 8, 219
- Turatto, M., Benetti, S., Cappellaro, E., Danziger, I. J., Della Valle, M., Gouiffes, C., Mazzali, P. A., & Patat, F. 1996, *MNRAS*, 283, 1
- Wang, L., Baade, D., & Patat, F. 2007, *Science*, 315, 212
- Wells, L. A., Phillips, M. M., Suntzeff, B., Heathcote, S. R., Hamuy, M., Navarrete, M., Fernandez, M., Weller, W. G., Schommer, R. A., Kirshner, R. P., Leibundgut, B., Willner, S. P., Peletier, S. P., Schlegel, E. M., Wheeler, J. C., Harkness, R. P., Bell, D. J., Matthews, J. M., Filippenko, A. V., Shields, J. C., Richmond, M. W., Jewitt, D., Luu, J., Tran, H. D., Appleton, P. N., Robson, E. I., Tyson, J. A., Guhathakurta, P., Eder, J. A., Bond, H. E., Potter, M., Veilleux, S., Porter, A. C., Humphreys, R. M., Janes, K. A., Williams, T. B., Costa, E., Ruiz, M. T., Lee, J. T., Lutz, J. H., Rich, R. M., Winkler, P. F., & Tyson, N. D. 1994, *AJ*, 108, 2233
- Younger, P. F. & van den Bergh, S. 1985, *A&AS*, 61, 365

TABLE I  
 PHOTOMETRIC AND HOST-GALAXY INFORMATION

SN Name	Host Galaxy	$\mu$ (mag)	Method <sup>a</sup>	$\mu$ Ref	Date of $B$ Maximum (JD-2,400,000)	$V_{\max}$ (mag)	$\Delta m_{15}(B)$	$\Delta$	$A_V$ (mag)	Phot Ref
SN 1980N	NGC 1316	31.50 (0.17)	SBF	1	44585.38 (0.35)	12.459 (0.034)	1.076 (0.089)	0.010 (0.030)	0.307 (0.044)	2
SN 1981B	NGC 4536	30.87 (0.04)	C	3	44670.95 (0.43)	11.954 (0.033)	1.009 (0.088)	-0.085 (0.035)	0.353 (0.074)	4,5
SN 1982B	NGC 2268	...	...	...	45012.91 (1.06)	13.333 (0.046)	0.940 (0.105)	-0.190 (0.060)	0.143 (0.125)	6
SN 1983G	NGC 4753	31.70 (0.19)	SBF	7	45429.72 (0.68)	12.669 (0.036)	1.093 (0.092)	0.063 (0.081)	0.924 (0.103)	8,9
SN 1986G	NGC 5128	27.96 (0.14)	SBF	7	46561.43 (0.13)	11.399 (0.065)	1.626 (0.135)	1.099 (0.036)	2.313 (0.101)	10
SN 1989B	NGC 3627	30.01 (0.08)	C	3	47564.27 (0.41)	11.993 (0.036)	1.066 (0.091)	0.046 (0.063)	1.457 (0.070)	11
SN 1989M	NGC 4579	...	...	...	...	...	...	...	...	...
SN 1990M	NGC 5493	...	...	...	...	...	...	...	...	...
SN 1990N	NGC 4639	31.71 (0.08)	C	3	48081.86 (0.08)	12.738 (0.035)	0.890 (0.091)	-0.253 (0.023)	0.245 (0.049)	12
SN 1991T	NGC 4527	30.61 (0.09)	C	13	48374.16 (0.07)	11.493 (0.034)	0.871 (0.089)	-0.279 (0.016)	0.337 (0.037)	14,15
SN 1991bg	NGC 4374 (M 84)	31.16 (0.05)	SBF	7	48602.91 (0.20)	11.913 (0.101)	0.871 (0.089)	1.409 (0.026)	0.467 (0.065)	16,17,18
SN 1992A	NGC 1380	31.07 (0.18)	SBF	1	48640.63 (0.11)	12.578 (0.032)	1.362 (0.088)	0.450 (0.028)	0.016 (0.011)	15,19
SN 2001ay	IC 4423	35.57 (0.15)	HF	20	52023.71 (0.49)	16.588 (0.034)	0.759 (0.088)	-0.441 (0.026)	0.338 (0.055)	21
SN 2001ba	MCG -05-28-001	35.55 (0.15)	HF	20	52034.21 (0.27)	16.551 (0.046)	1.014 (0.105)	-0.116 (0.029)	0.016 (0.012)	22
SN 2001eh	UGC 1162	35.92 (0.15)	HF	20	52169.56 (0.19)	16.815 (0.045)	0.830 (0.104)	-0.307 (0.020)	0.024 (0.016)	23
SN 2001el	NGC 1448	...	...	...	52182.13 (0.08)	12.713 (0.033)	0.995 (0.087)	-0.090 (0.020)	0.745 (0.040)	24
SN 2001ep	NGC 1699	...	...	...	52200.10 (0.08)	14.989 (0.040)	1.109 (0.097)	0.057 (0.026)	0.568 (0.056)	23
SN 2001ex	UGC 3595	35.24 (0.15)	HF	20	52204.80 (0.24)	17.324 (0.041)	1.695 (0.099)	1.006 (0.083)	0.415 (0.148)	23
SN 2003bf	2MASX J08082660+1219571	35.81 (0.15)	HF	20	...	...	...	...	...	...
SN 2003bt	MCG -01-28-006	35.34 (0.15)	HF	20	...	...	...	...	...	...

REFERENCES. — (1) Jensen et al. 2003; (2) Hamuy et al. 1991; (3) Freedman et al. 2001; (4) Buta & Turner 1983; (5) Tsvetkov 1982; (6) Ciatti et al. 1988; (7) Tonry et al. 2001; (8) Buta et al. 1985; (9) Younger & van den Bergh 1985; (10) Phillips et al. 1987; (11) Wells et al. 1994; (12) Lira et al. 1998; (13) Gibson et al. 2000; (14) Lira et al. 1998; (15) Altavilla et al. 2004; (16) Filippenko et al. 1992a; (17) Leibundgut et al. 1993; (18) Turatto et al. 1996; (19) N. Suntzeff 2005, private communication; (20) NASA/IPAC Extragalactic Database; (21) K. Krisciunas 2005, private communication; (22) Krisciunas et al. 2004; (23) Ganeshalingam et al. 2008; (24) Krisciunas et al. 2003.

NOTE. — Uncertainties are given in parentheses.

<sup>a</sup> Method of determining distance modulus — C = Cepheid variable stars; SBF = surface brightness fluctuations; HF = Hubble flow.

TABLE 2  
 SPECTROSCOPIC INFORMATION

SN Name	UT Date yyyy-mm-dd	Telescope / Instrument	Phase (d)	Fe II Velocity ( $10^3 \text{ km s}^{-1}$ )	Fe II EW ( $\text{\AA}$ )	UV Ratio $\mathcal{R}_{UV}$
SN 1980N	1980-12-11.724	<i>IUE</i>	-0.2	18.2	58.2	0.28 (0.02)
SN 1980N	1980-12-13.495	<i>IUE</i>	1.6	21.6	69.6	0.29 (0.03)
SN 1980N	1980-12-16.147	<i>IUE</i>	4.2	16.8	80.3	0.34 (0.04)
SN 1980N	1980-12-17.712	<i>IUE</i>	5.8	23.5	10.2	0.41 (0.04)
SN 1980N	1980-12-23.371	<i>IUE</i>	11.4	23.5	17.0	0.58 (0.05)
SN 1980N	1980-12-24.831	<i>IUE</i>	12.9	24.5	11.8	0.59 (0.04)
SN 1980N	1981-01-16.810	<i>IUE</i>	35.7	22.0	55.9	0.90 (0.09)
SN 1981B	1981-03-09.295	<i>IUE</i>	1.8	20.6	47.3	0.32 (0.01)
SN 1981B	1981-03-10.460	<i>IUE</i>	3.0	21.4	49.0	0.27 (0.02)
SN 1981B	1981-03-11.597	<i>IUE</i>	4.1	...	...	0.53 (0.06)
SN 1982B	1982-02-18.436	<i>IUE</i>	6.0	20.2	27.2	...
SN 1983G	1983-04-08.481	<i>IUE</i>	3.2	20.1	44.0	0.53 (0.03)
SN 1983G	1983-04-09.368	<i>IUE</i>	4.1	...	...	0.45 (0.15)
SN 1983G	1983-04-11.544	<i>IUE</i>	6.3	19.5	20.5	0.44 (0.03)
SN 1983G	1983-04-14.281	<i>IUE</i>	9.0	20.8	56.3	0.56 (0.02)
SN 1983G	1983-04-19.569	<i>IUE</i>	14.3	19.7	56.7	0.27 (0.05)
SN 1983G	1983-04-25.289	<i>IUE</i>	20.0	21.7	67.9	0.54 (0.03)
SN 1986G	1986-05-06.685	<i>IUE</i>	-4.2	...	...	0.51 (0.18)
SN 1986G	1986-05-08.146	<i>IUE</i>	-2.8	28.6	42.9	0.45 (0.08)
SN 1986G	1986-05-12.493	<i>IUE</i>	1.6	21.4	71.1	0.39 (0.02)
SN 1986G	1986-05-15.138	<i>IUE</i>	4.2	...	...	0.46 (0.03)
SN 1986G	1986-05-19.321	<i>IUE</i>	8.4	25.1	47.7	0.42 (0.09)
SN 1986G	1986-05-29.301	<i>IUE</i>	18.3	20.9	79.2	0.88 (0.08)
SN 1989B	1989-02-01.480	<i>IUE</i>	-5.3	20.2	19.7	0.43 (0.01)
SN 1989M	1989-07-06.988	<i>IUE</i>	...	20.0	62.4	...
SN 1989M	1989-07-08.569	<i>IUE</i>	...	19.5	49.5	...
SN 1989M	1989-07-12.735	<i>IUE</i>	...	18.8	42.0	...
SN 1989M	1989-07-14.058	<i>IUE</i>	...	17.7	34.6	...
SN 1989M	1989-07-17.730	<i>IUE</i>	...	15.1	39.8	...
SN 1989M	1989-07-20.034	<i>IUE</i>	...	16.9	37.8	...
SN 1990M	1990-06-15.836	<i>IUE</i>	...	23.1	24.5	...
SN 1990M	1990-06-18.493	<i>IUE</i>	...	23.0	16.9	...
SN 1990N	1990-06-26.817	<i>IUE</i>	-12.5	...	...	0.41 (0.02)
SN 1990N	1990-06-28.391	<i>IUE</i>	-11.0	28.8	63.6	0.60 (0.06)
SN 1990N	1990-06-30.726	<i>IUE</i>	-8.6	27.5	37.9	0.41 (0.01)
SN 1990N	1990-07-02.727	<i>IUE</i>	-6.6	30.8	30.6	0.35 (0.03)
SN 1990N	1990-07-04.333	<i>IUE</i>	-5.0	32.6	42.2	0.35 (0.01)
SN 1990N	1990-07-09.730	<i>IUE</i>	0.3	24.2	17.4	0.29 (0.01)
SN 1990N	1990-07-14.301	<i>IUE</i>	4.9	21.6	23.9	0.37 (0.01)
SN 1991T	1991-04-27.424	<i>IUE</i>	-0.1	22.3	16.9	0.26 (0.01)
SN 1991T	1991-04-29.672	<i>IUE</i>	2.1	21.7	20.7	0.23 (0.01)
SN 1991bg	1991-12-14.824	<i>IUE</i>	2.4	...	...	...
SN 1992A	1992-01-14.083	<i>IUE</i>	-5.0	20.4	45.1	0.33 (0.01)
SN 1992A	1992-01-16.220	<i>IUE</i>	-2.9	20.7	49.7	0.41 (0.03)
SN 1992A	1992-01-18.952	<i>IUE</i>	-0.2	19.2	51.5	0.36 (0.02)
SN 1992A	1992-01-21.574	<i>IUE</i>	2.4	18.6	61.4	0.37 (0.01)
SN 1992A	1992-01-24.214	<i>HST/FOS</i>	5.1	19.1	55.0	0.45 (0.03)
SN 1992A	1992-01-27.666	<i>IUE</i>	8.5	21.4	49.0	0.53 (0.02)
SN 1992A	1992-01-30.906	<i>IUE</i>	11.7	21.5	61.3	0.60 (0.01)
SN 1992A	1992-02-04.218	<i>IUE</i>	16.0	...	...	0.78 (0.03)
SN 1992A	1992-02-10.659	<i>IUE</i>	22.4	...	...	1.08 (0.12)
SN 1992A	1992-03-04.310	<i>HST/FOS</i>	44.9	...	...	0.87 (0.02)
SN 1992A	1992-11-05.592	<i>HST/FOS</i>	289.7	...	...	0.55 (0.06)
SN 2001ay	2001-05-02.813	<i>HST/STIS</i>	8.3	19.3	21.5	...
SN 2001ay	2001-05-09.704	<i>HST/STIS</i>	15.0	19.2	30.1	...
SN 2001ba	2001-05-08.791	<i>HST/STIS</i>	4.0	19.3	48.5	...
SN 2001ba	2001-05-16.229	<i>HST/STIS</i>	11.2	18.0	47.4	...
SN 2001eh	2001-09-25.757	<i>HST/STIS</i>	8.1	...	...	0.33 (0.01)
SN 2001eh	2001-10-04.523	<i>HST/STIS</i>	16.6	26.4	48.3	0.49 (0.02)
SN 2001el	2001-10-29.636	<i>HST/STIS</i>	29.9	18.3	28.8	...
SN 2001el	2001-11-06.569	<i>HST/STIS</i>	37.8	17.2	39.9	...
SN 2001el	2001-11-13.476	<i>HST/STIS</i>	44.7	15.9	42.4	...
SN 2001el	2001-11-20.356	<i>HST/STIS</i>	51.5	18.6	46.2	...
SN 2001el	2001-11-26.704	<i>HST/STIS</i>	57.8	18.6	40.9	...
SN 2001el	2001-12-04.350	<i>HST/STIS</i>	65.5	15.5	55.2	...
SN 2001ep	2001-10-28.024	<i>HST/STIS</i>	10.3	...	...	...
SN 2001ep	2001-11-02.871	<i>HST/STIS</i>	16.1	...	...	...
SN 2001ex	2001-10-29.475	<i>HST/STIS</i>	7.0	23.1	...	...
SN 2001ex	2001-11-06.424	<i>HST/STIS</i>	14.7	...	...	...
SN 2001ex	2001-11-12.786	<i>HST/STIS</i>	20.9	...	...	...
SN 2001ex	2001-11-19.272	<i>HST/STIS</i>	27.3	...	...	...
SN 2001ex	2001-11-26.885	<i>HST/STIS</i>	34.7	...	...	...
SN 2001ex	2001-12-03.964	<i>HST/STIS</i>	41.6	...	...	...

TABLE 2 — *Continued*

SN Name	UT Date yyyy-mm-dd	Telescope / Instrument	Phase (d)	Fe II Velocity ( $10^3 \text{ km s}^{-1}$ )	Fe II EW ( $\text{\AA}$ )	UV Ratio $\mathcal{R}_{UV}$
SN 2003bf	2003-03-10.836	<i>HST</i> /STIS	...	17.0	42.6	...
SN 2003bf	2003-03-17.577	<i>HST</i> /STIS	...	...	...	...
SN 2003bf	2003-03-24.245	<i>HST</i> /STIS	...	...	...	...
SN 2003bf	2003-03-17.713	<i>HST</i> /STIS	...	...	...	...

NOTE. — Uncertainties are given in parentheses.